Osteoarthritis and Cartilage 31 (2023) 49–59

Osteoarthritis and Cartilage

OARSI OSTEOARTHRITIS RESEARCH SOCIETY INTERNATIONAL

Changes of the subchondral bone microchannel network in early osteoarthritis

S. Taheri † *, T. Yoshida †, K.O. Böker †, R.H. Foerster †, L. Jochim †, A.L. Flux ‡, B. Grosskopf ‡, T. Hawellek †, W. Lehmann †, A.F. Schilling †

† *Department of Trauma Surgery, Orthopaedic Surgery and Plastic Surgery, University Medical Center Göttingen, Göttingen, Germany*
‡ *University of Göttingen Johann-Friedrich-Blumenbach-Institute for Zoology # Anthropology, Department of Historical Anthropology and Human Ecology, Göttingen, Germany*

ARTICLE INFO

Article history:
Received 19 April 2022
Accepted 4 October 2022

Keywords:
Bone microarchitecture
Osteoarthritis
Cartilage-bone marrow microchannel connectors
Human femoral head
Subchondral bone
Bone micro-CT

SUMMARY

Objective: We have identified a 3D network of subchondral microchannels that connects the deep zone of cartilage to the bone marrow (i.e., cartilage-bone marrow microchannel connectors; CMMC). However, the pathological significance of CMMC is largely unknown. Here, we quantitatively evaluated how the CMMC microarchitecture is related to cartilage condition, as well as regional differences in early idiopathic osteoarthritis (OA).

Methods: Two groups of cadaveric female human femoral heads (intact cartilage vs early cartilage lesions) were identified, and a biopsy-based high-resolution micro-CT imaging was employed. Subchondral bone (SB) thickness, CMMC number, maximum and minimum CMMC size, and the CMMC morphology were quantified and compared between the two groups. The effect of joint's region and cartilage condition was examined on each dependent variable.

Results: The CMMC number and morphology were affected by region of the joint, but not by cartilage condition. On the other hand, the minimum and maximum CMMC size was changed by both the location on the joint, as well as the cartilage condition. The smallest CMMC were consistently detected at the load-bearing region (LBR) of the joint. Compared to non-pathological subjects, the size of the microchannels was enlarged in early OA, most noticeably at the non-load-bearing region (NLBR) and the peripheral rim (PR) of the femoral head. Furthermore, subchondral bone thinning was observed in early OA as a localized occurrence linked with areas of partial chondral defect.

Conclusion: Our data point to an enlargement of the SB microchannel network, and a collective structural deterioration of SB in early idiopathic OA.

Introduction

Osteoarthritis (OA) is a prevalent joint disorder with an increasing public health challenge that profoundly impacts individuals as well as the society in general[1]. Although originally labeled as a "wear and tear" process mainly characterized by articular cartilage (AC) degradation, OA is now widely considered to be a progressive joint failure involving all periarticular tissues[2,3]. In particular, there is growing evidence that subchondral bone (SB) plays a crucial role in the initiation and progression of OA[4,5].

AC and SB are intimately interlocked, creating a complex unit called the AC-SB interface, where the functionality and homeostasis of the adjacent unit can be modulated by mediators from the other tissue[6,7]. Through the course of bone remodeling, leukotrienes, prostaglandins, and several growth factors that are released *in vivo* by osteoblasts can reach the overlying cartilage[8]. Conversely, inflammatory and osteoclast stimulation factors released by chondrocytes can lead to subchondral bone deterioration[9,10]. However, the direct connective pathways allowing this communication between AC and SB are poorly understood. Since the second half of the last century, smaller fractures or microchannels in subchondral bone were observed[11–14]. Our recent studies have revealed that

* Address correspondence and reprint requests to: S. Taheri, Department of Trauma Surgery, Orthopaedic Surgery and Plastic Surgery, Universitätsmedizin Göttingen, Robert-Koch-Str. 40, 37075 Göttingen, Germany. Tel.: 49-(0)-551-39-62613.
E-mail address: shahed.taheri@med.uni-goettingen.de (S. Taheri).

https://doi.org/10.1016/j.joca.2022.10.002

Abbreviations

AC	Articular cartilage
SB	Subchondral bone
CMMC	Cartilage-bone marrow microchannel connectors
OA	Osteoarthritis
LBR	Load-bearing region
NLBR	Non-load-bearing region
PR	Peripheral rim
CC	Calcified cartilage
MHH	Medizinische Hochschule Hannover
SI	Supporting Information
Micro-CT	Microcomputed Tomography
Circ.	Circularity index
Feret	Maximum caliper dimeter
MinFeret	Minimum caliper dimeter
GMM	Generalized estimating equation
SEM	The standard error of the mean
WCS	Wald Chi-square
WCI	Wald Confidence Interval

cartilage and bone marrow are connected by a three-dimensional network of microchannels (i.e., cartilage-bone marrow microchannel connector; CMMC), which are microarchitecturally different in number, size, and morphology depending on the maturation phase of the bone[15], as well as the region of the joint[16,17]. Despite the potentially strong implications that these CMMCs can have on cartilage nutrition[14,18], biochemical bone-cartilage crosstalk[19], and even on the biomechanical deformability of subchondral bone[20], there is surprisingly a lack of studies on their (patho)physiological significance. In normal human femoral heads, the age-related reduction of vessel-containing SB perforations has been interpreted as an early degeneration marker[21], while direct contact of capillaries with the deep zone of cartilage in adult joints has been considered a remodeling process[22,23]. Given our recent findings on the CMMC network, and accumulating evidence that the (micro)structural changes of SB precede full-focal cartilage defects[24,25], one essential question is if/how these hierarchical microarchitectures change in early OA.

Here, we extended our established methodology to quantitatively evaluate the CMMC network of human femoral heads that exhibit partial-thickness defects and mild chondral fibrillations associated with idiopathic early OA. We hypothesized that the CMMC metrics change based on the health-state of the overlying cartilage, as well as areas of the joint that represent regional differences in physiological loading.

Materials and methods

Preparation and selection criteria of human bone specimens

The subjects used in this study were anonymous human femurs granted by the anatomical gift program of the Hannover Medical School (MHH). As no information was provided regarding the medical history, sex, and age of the cadaver donors, the OA status, sex, and the biological age of the subjects were determined post-mortem as outlined in Section 1 of the Supporting Information (SI). Five healthy and five early arthritic female donors (right leg) were selected for measurement and analysis. The majority of subjects had a biological age of 40–60 years at death (Table S2).

Assigning of the measuring points and biopsy

To acquire high-resolution images, 2.00-mm cartilage-bone cylinders were extracted from the surface of femoral heads. In healthy subjects, the measuring points were intersections of twelve concentric lines and four parasagittal planes that were outlined on the surface of the joint using a template grid [Fig. 1(A); details in Ref.16]. 43 measuring points were extracted from the surface of each healthy subject [215 biopsies in total; yellow dots in Fig. 1(B)]. These geometrical shapes divide each femoral head into several sectors, one of which is marked by black crosshatched lines in Fig. 1(B). A maximum of four measuring points per sector was extracted from early OA subjects in case the entire surface of the sector was covered by early chondral defects. With the aid of a template grid that incorporated the described shapes, the position of each set of biopsy was standardized taking into consideration the normalized size of each joint. Additionally, a severity mapping of local partial-thickness defects was created by a sequence that comprised several photogrammetry procedures [Fig. 1(C)–(E); details in the SI]. In total, 116 cartilage-bone biopsies were drilled out and scanned from regions where the overlying cartilage showed early pathological features, and compared with the 215 biopsies of healthy femurs.

Micro-CT acquisition and data analysis

Micro-CT settings and measurement techniques are identical to our previous study, where the 215 biopsies of healthy femurs were evaluated[16]. The SB thickness was measured in sagittal cross-sections of the 3D-reconstructed models, while the CMMC metrics were quantified on a layer-by-layer basis (in the transverse plane relative to the long axis of the biopsy) using an ImageJ macro. They were characterized by their local density per mm^2 (CMMC number), maximum (Feret) and minimum size (MinFeret), as well as the morphological index, Circularity (Circ.[16]). For schematic descriptions and exemplary values of Feret, MinFeret, and Circ., see Fig. S3.

By estimating reaction forces at the right hip from the gait analysis on a separate healthy cohort, we have previously demonstrated that regional differences in the microchannel architecture of SB may reflect regional differences in loading[16]. The results were used as a physiological reference to categorize the output of the algorithm (i.e., CMMC metrics). Similarly, the results here are categorized and reported for the identical load-bearing region (LBR), non-load-bearing region (NLBR), and the peripheral rim of the joint (PR; see middle panel in Fig. 4). The number of measuring points for each region and health-states are reported in Table I.

Statistics

We evaluated the effect of region and cartilage condition on SB thickness and each CMMC metric using generalized estimating equation (GEE) models. A detailed description of the methods, including statistical analyses and histological techniques is provided in the SI.

Results

Early subchondral thinning and cartilage fibrillation occur prevalently at the inferoposterior portion of the femoral head

The SB thickness measurements indicated a strong effect of region (95% Wald Confidence Interval; 95% WCI = 87.13 to 169.46, $p < 0.0001$). Irrespective of the health-status of the cartilage, the thickest subchondral bone was detected at LBR of the femoral head (mean = 239.41 μm, SEM = 14.90, 95% WCI = 210.21 to 268.61),

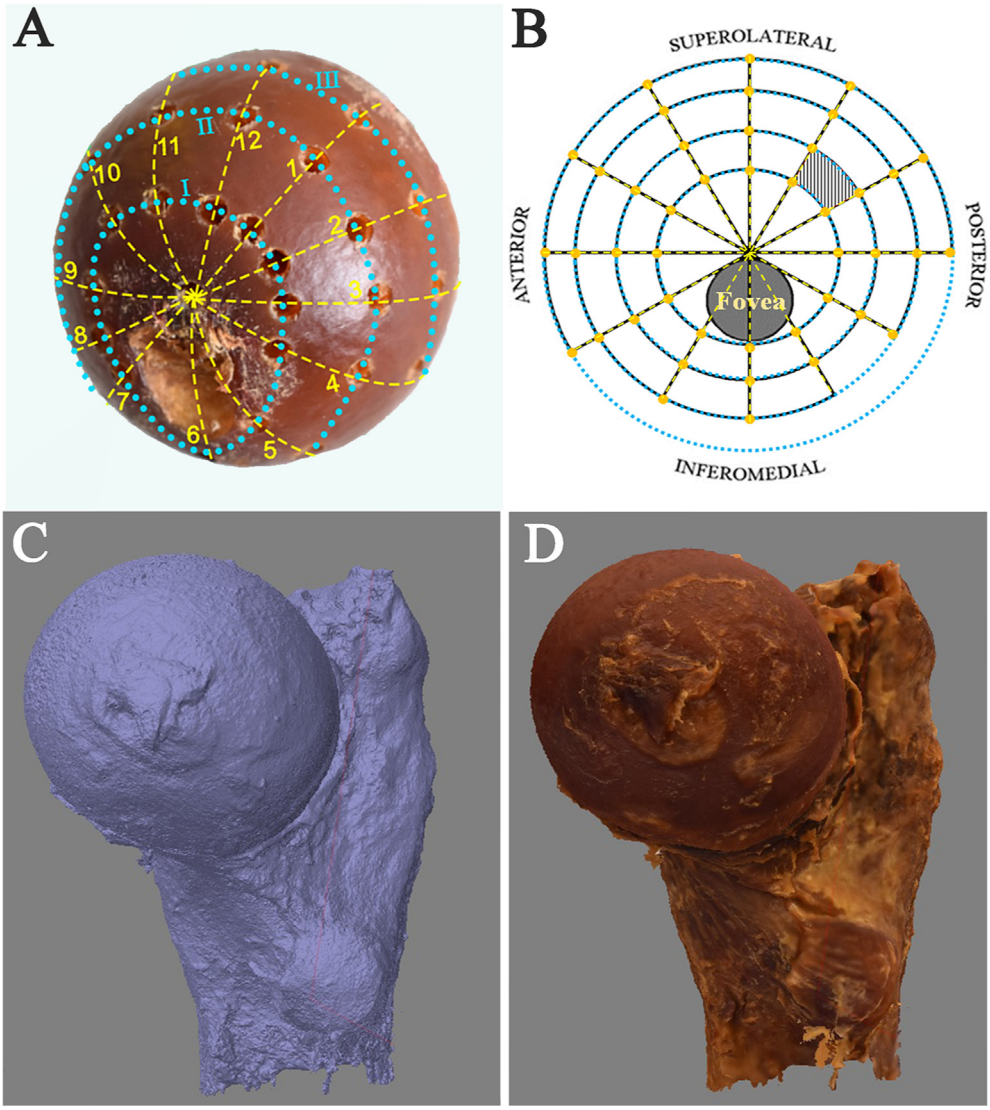

Fig. 1

Osteoarthritis and Cartilage

The system for assigning measuring points on the femoral head. (*A*) For healthy subjects, measuring points were defined as the convergence points of twelve concentric lines (yellow dashed lines) and four parallel parasagittal planes (Roman numerals; cyan) on the surface of the joint. (*B*) In each healthy subject, 43 cartilage-bone cylinders were extracted for high-resolution scanning from the designated locations (orange dots). The aforementioned geometrical shapes divided each femoral head into 42 sectors, one of which was marked by black crosshatched lines. For early OA subjects, 1–4 biopsies per sector were extracted and scanned depending on the expansion of early OA cartilage characteristics (i.e., partial-thickness defects and fibrillations) over each individual sector. To create a severity mapping of the most prevalent early OA regions of the joint, areas of early cartilage degeneration were superimposed by a photogrammetry technique that consisted of photo alignment and point cloud generation. (*C*) processing of dense could and continuous mesh over the surface of the model, and (*D*) integration of the texture maps over each mesh to generate realistic 3D models of each subject.

while the SB thickness was significantly reduced at NLBR ($\beta = -82.52$, 95% WCI for difference $= -121.13$ to -43.93, $P = 0.005$), and the peripheral rim ($\beta = -107.58$, 95% WCI for difference $= -139.04$ to -76.15, $p < 0.0001$) of the joint [Fig. 2(A)]. We also observed a milder, albeit significant effect of cartilage condition on SB thickness (95% WCI = 4.99 to 66.76, $p = 0.023$). At the LBR, the SB thickness was not affected by cartilage condition (mean difference = 4.90, 95% CI for difference = −82.55 to 92.35). Pairwise comparisons, however, showed that early OA subchondral thinning was detected at the NLBR (mean difference = 56.435; 95% WCI for difference = 16.8129 to 96.0571; $p = 0.004$). At the rim, a trend toward the reduction of SB thickness was observed, which was not significant (95% WCI for difference = −6.598 to 99.214; $P = 0.153$).

The colormap of partial thickness defect showed that early cartilage lesions and fibrillations were most prevalent

Investigated bone	OA status	No. of measuring points		
		LBR	NLBR	PR
Subject 1	healthy	12	12	19
Subject 2	healthy	12	12	19
Subject 3	healthy	12	12	19
Subject 4	healthy	12	12	19
Subject 5	healthy	12	12	19
Subject 6	Early OA	0	10	8
Subject 7	Early OA	0	10	3
Subject 8	Early OA	4	21	14
Subject 9	Early OA	2	16	2
Subject 10	Early OA	5	16	5

Table I Osteoarthritis and Cartilage

Measuring point allocation per subject

inferoposteriorly in the vicinity of the fovea capitis [Fig. 2(B)]. Consequently, the majority of early OA measuring points were located at the NLBR (63%), and the outermost PR of the joint (27.6%), while the least frequency of partial thickness defect (9.4%) was observed at the load-bearing, anterosuperior portion of the joint.

Masson-Goldner's trichrome staining of the osteochondral junction supported our macroscopic observations and sample selection. Healthy subjects were characterized by a regular cartilage surface, as well as a hierarchical chondrocyte distribution in different cartilage zones [Fig. 2(C)]. CMMCs could occasionally be detected as two-dimensional vessels in the sagittal plane [one of which is magnified image in Fig. 2(D)]. They advanced through the calcified cartilage layer at the contact point of cartilage and subchondral bone, and were surrounded by the subchondral bone plate. On the other hand, the early OA biopsies were signified by cartilage erosion and partial thickness defects down to the mid-zone of cartilage as expected [Fig. 2(E)], a loss of morphological variation in chondrocytes in different cartilage zones, tidemark duplication, and discoloration at the uppermost cartilage surface due to ectopic cartilage calcification [Fig. 2(F)].

Histological examination of the CMMC network in transverse cuts

An exemplary microCT-acquired 2D image and the corresponding binarized image is depicted [Fig. 3(A) and (B)]. Two neighbor transverse cuts from the same cross-section of the biopsy were stained by Giemsa and Masson-Goldner trichrome [Fig. 3(C) and (D), respectively], revealing identical microporous structures compared to the micro-CT image, which demonstrated the utility of transverse cuts for histological examination of the CMMC network, as well the accuracy of the applied threshold setting in micro-CT analysis. Most CMMCs were surrounded by a concentric sheath of appositional lamellar bone that did not comprise an endosteum, and therefore, seemed to be different from classic mature osteons. Additionally, the microchannels contained thin-walled vessel-like membranes that were lined with intravascular-, as well as extravascular cells in the encompassing subchondral bone plate (higher magnification images in Fig. S6). The exact cellular and molecular contents of the CMMCs are unknown, even though morphological assessments strongly indicated that SB microchannels were composed of diverse microvasculature structures (see Section 4 of the SI).

General overview of the regional CMMC characteristics based on the health-status of the overlying cartilage

The representative 3D-reconstructed models showed that the region-specific distribution of the microchannels that we previously observed in the healthy, control group persisted in early-OA group as well[16]. i.e., In the LBR, SB in both healthy and early OA subjects is perfused with abundant small microchannels, which form several coalescent finger-like interconnections [Fig. 4(A); Supplemental Videos 1 and 2]. On the other hand, NLBR is characterized by sporadic ampulla-like canals with a varying combination of small, medium, and large channel sizes [Fig. 4(B); Supplemental Videos 3 and 4]. The largest CMMCs are typically detected at the PR of the joint as irregularly-shaped gap formations with sizeable contact areas with cartilage [~0.003–0.012 mm^2; Fig. 4(C); Supplemental Videos 5 and 6]. Observations indicated that the CMMC size was generally larger in early OA subjects compared to their region-specific healthy counterparts [Fig. 4(A)–(C)].

Supplementary video related to this article can be found at https://doi.org/10.1016/j.joca.2022.10.002.

To demonstrate the intricate microstructure of the CMMCs, an exemplary model was virtually cut and viewed from an arbitrary coronal plane [yellow dash line in Fig. 4(A), viewed in Fig. 4(D)], which revealed isolated microporous structures in the plane of sectioning. Nonetheless, the inverted 3D-representation showed that these micropores were part of a dense CMMC network that existed throughout the entire subchondral bone.

The local density of CMMC does not change in early OA but their size is increased

The type III test of model effects revealed no effect of the joint's cartilage condition on the CMMC number (95% WCI = −2.703 to 3.585, $P = 0.883$), but a significant impact of region (95% WCI = 5.669–8.464, $P < 0.0001$). The estimated marginal means, SEM, and the 95% WCI of all the CMMC metrics across the levels of each factor are presented in Table II. Irrespective of cartilage condition, the CMMC number was lower in the NLBR (β regression coefficient = −4.486, 95% WCI for difference = −6.567 to −3.684, $P < 0.0001$), and the PR ($\beta = -5.381$, 95% WCI for difference = −6.648 to −3.637, $P < 0.0001$) compared to the LBR as reference. In early OA samples, in particular, a consistently higher CMMC number was detected in the LBR than the NLBR (95% WCI for difference = 3.162 to 5.809; $P = 0.036$) and the PR (95% WCI for difference = 4.789 to 5.974; $P < 0.01$). Other significant pairwise comparisons are marked in Fig. 5(A).

For the maximum size of the microchannels, it was observed that both cartilage condition (95% WCI = 8.682–31.770, $P = 0.002$) and region (95% WCI = 64.198 to 86.330, < 0.0001) had significant effects on the Feret diameter. Compared to the non-pathological subjects, the maximum diameter of early OA microchannels were enlarged in all regions; Namely, 36.7% (mean difference = 20.226; 95% WCI for difference = 2.938 to 37.514; $P = 0.018$), 77.1% (mean difference = 57.271; 95% WCI for difference = 33.234 to 81.308; $P = 0.0009$) and 78.8% (mean difference = 71.953; 95% WCI for difference = 21.8775 to 122.0295; $P < 0.01$) increases were observed in the LBR, NLBR, and the PR, respectively. Interestingly, the spread around the Feret's population means were wider in early OA (i.e., higher standard of error) compared to the non-pathological group [Fig. 5(B)]. Regardless of the health status of the cartilage, the smallest microchannels were consistently detected at the LBR of the femoral head, while the CMMCs were significantly larger in the NLBR ($\beta = 37.79$, $p < 0.0001$), and the rim ($\beta = 62.12$, $p < 0.0001$) of the joint. The distribution difference of Feret between NLBR and PR was narrower, but significant nevertheless ($\beta = 24.32$, $p = 0.023$).

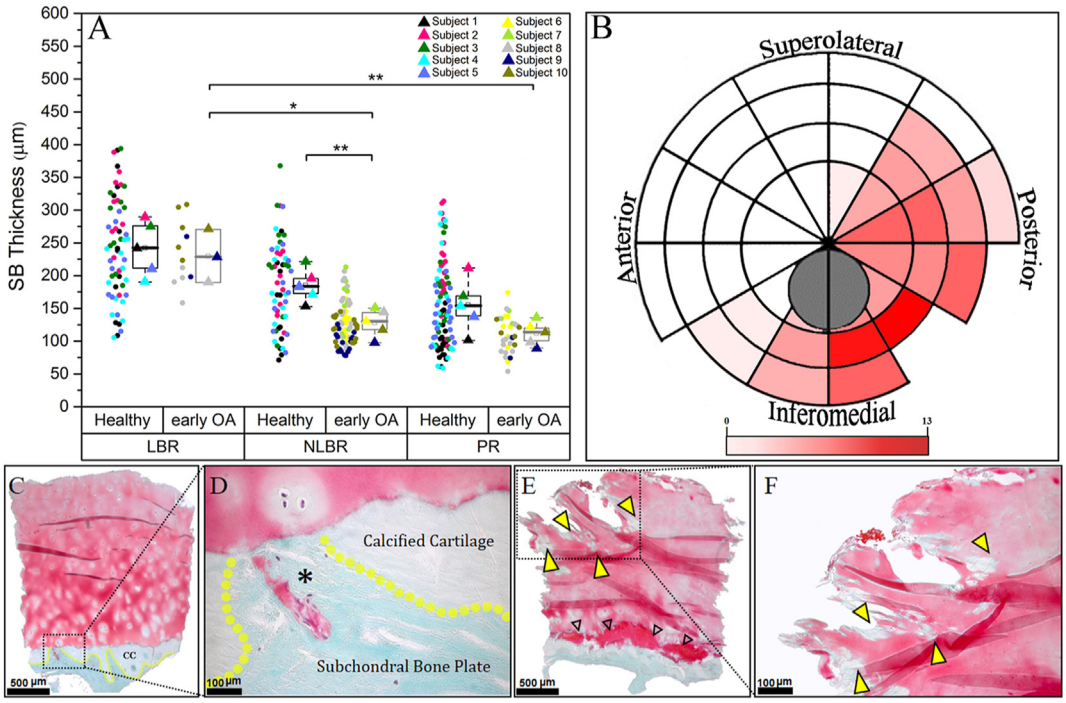

Fig. 2

Osteoarthritis and Cartilage

Changes of SB thickness and characteristics of early cartilage defects in human femoral head. (*A*) Changes of SB thickness in different areas of the femoral head. Data are presented as box plots with whiskers. The triangles overlying the boxplots signify the mean values of corresponding subjects in each region and cartilage condition. Subjects 1–5 were healthy while subjects 6–10 had early osteoarthritic chondral characteristics ($n = 5$ per group). Each circle in close proximity to the boxplots represent the mean value of a measuring point, color-coded to its corresponding subject (**m**; number of measuring points = 215 for healthy subjects; 116 for early OA subjects). Analysis was conducted using generalized estimating equation followed by the Bonferroni test for pairwise comparison. Significant *P*-values are presented as $^*P < 0.05$; $^{**}P < 0.01$. (*B*) Colormap of the distribution of early cartilage lesions in five subjects with a mean Outerbridge score between 1.5 and 2.5. The color scale is based on the total number of measuring points per sector in the five subjects, where a maximum of four measuring points per sector was extracted in case the entire surface of the sector was covered by early OA chondral defects. (*C*) Masson-Goldner staining of a representative sagittal section of a healthy biopsy showed a preserved articular surface with no signs of cartilage degradation, a zone-dependent chondrocyte distribution, and a single microchannel with an approximate size of 25 µm. (*D*) The microchannel (marked by asterisk) was engulfed by a sheath of subchondral bone lamellae (turquoise), which penetrated through the calcified cartilage layer (CC; pale green). (*E*) In early osteoarthritic cartilage, partial degradation of the superficial cartilage layer was observed, tidemark duplication was detected (open triangles), and chondrocytes lost their hierarchical distribution within the extracellular cartilage matrix. Additionally, cartilage discoloration associated with ectopic cartilage calcification was found to be a prominent phenomenon (*F*; yellow triangles).

Similar observations were made for the influence of cartilage condition (95% WCI = 0.381 to 23.226, $p = 0.0045$) and region (95% WCI = 36.744 to 59.306, $p < 0.0001$) on the minimum CMMC caliper diameter. The MinFeret showed a clear increasing trend in early OA compared to the corresponding healthy groups, which was significant at the NLBR (mean difference = 37.81; 95% WCI for difference = 16.73 to 58.89; $p < 0.001$) and the PR (mean difference = 35.40; 95% WCI for difference = 13.11 to 57.70; $p = 0.0014$), but not significant at the LBR [$p = 0.64$; Fig. 5(C)]. Additionally, the MinFeret diameter was generally smallest at the LBR (the reference category in parameter estimation), and was progressively increased at the NLBR ($\beta = 23.31$, $p = 0.007$), and the PR ($\beta = 33.13$, $p < 0.0001$).

The morphology of the SB microchannels was impacted by the region (95% WCI = 0.74 to 0.844, $p < 0.0001$), but not by the cartilage condition (95% WCI = −0.017 to 0.098, $p = 0.078$). The CMMCs were generally round and circular in the LBR, while getting increasingly elongated and irregular at the NLBR ($\beta = -0.081$, 95% WCI for difference = −0.1136 to −0.0474, $p < 0.0001$), and especially the rim of the joint ($\beta = -0.131$, 95% WCI for difference = −0.1648 to −0.0969, $p < 0.0001$). Again, we found a higher variance in the early OA subjects compared to their healthy counterparts. In particular, the LBR measuring points were two times more spread out from the mean, and from one another (SEM: 0.026 vs 0.0126) compared to the healthy subjects. When early OA groups were compared to their respective healthy regions, decreasing trends were observed for all groups, which were, however, not significant (LBR: $p = 1.0$; NLBR: $p = 0.052$; PR: $p = 0.67$) owing to the aforementioned variance [Fig. 5(D)].

Discussion

OA is a leading cause of chronic pain and disability worldwide where early pathological changes occur well before the disease is

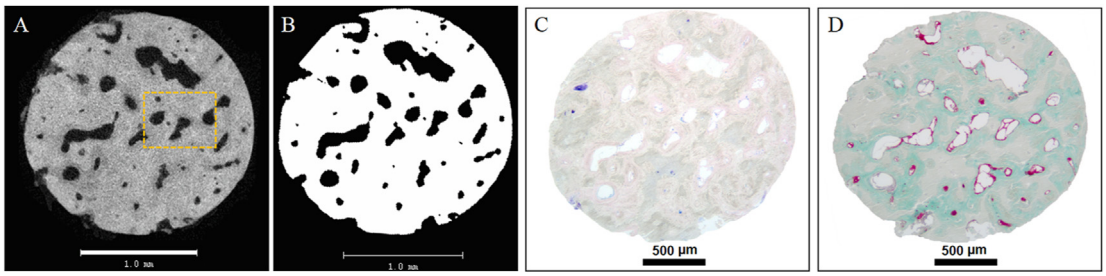

Fig. 3

Osteoarthritis and Cartilage

Histological examination of the CMMC network in transverse cuts. (*A*) a 2D slide of an exemplary biopsy obtained from micro-CT imaging before and (*B*) after segmentation and binarization. Transverse sectioning of histological cuts allow for a direct correlation between CMMC structures derived from micro-CT with corresponding histological slides. Two consecutive sections situated at ~100 μm below the tidemark were stained by (*C*) Giemsa and (*D*) Masson-Goldner's trichrome, showing identical microporous features to the micro-CT image, as well as a concentric lamellar bone structure that surrounds each CMMC. Higher magnification Alcian blue, Giemsa, and Masson-Goldner stainings of a selected region of interest (the dotted orange rectangle in *A*) are shown in Fig. S4(D–F) of the supporting information and illustrate more details.

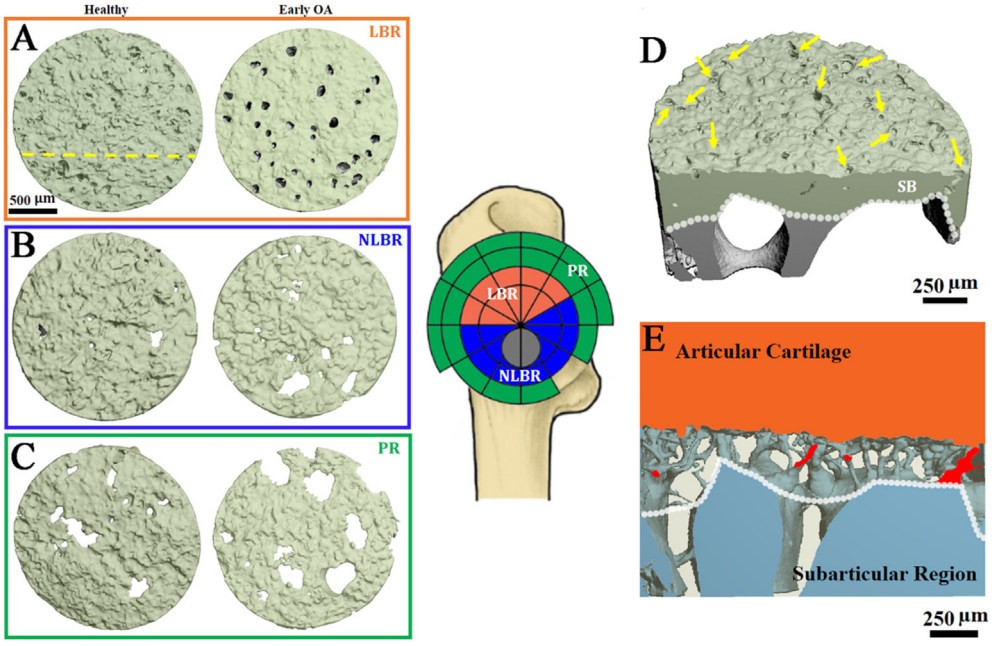

Fig. 4

Osteoarthritis and Cartilage

3D representation of the SB microchannel network in human femoral head. (*A*) The superior view of typical samples associated with the load-bearing region (LBR; marked in orange in the central figure) revealed abundant microchannels reaching to the uppermost superficial surface of SB. *(B)* At the non-load-bearing region of the joint (NLBR; marked in blue), the local density of the CMMC appeared to be reduced compared to the LBR with a varying combination of small and medium-sized channels, while (*C*) the peripheral rim of the joint (PR; marked in green) was characterized by large and irregularly-shaped gap formations in the SB. In each identified area, an enlargement of the CMMC size was observed in early arthritic biopsies compared to the corresponding healthy specimens (*A–C*). (*D*) The cross-section of the healthy, LBR model was cut at a random plane of sectioning (yellow dotted line in *A*). Yellow arrowheads signify selected CMMCs that reached the SB surface (E) The negative 3D model of the same LBR cross-section showed the AC in orange, osseous structures in transparent, and the CMMC in blue-grey. The micro-channels were visible throughout the entire thickness of the SB, while discrete microchannels cut by the random plane of sectioning were marked in red. The white dotted lines in *D* and *E* denote the lower margin of the subchondral bone plate.

CMMC metrics	Cartilage condition	Region	Mean	SEM (Std. Error)	95% Wald Confidence Interval	
					Lower	Upper
CMMC number [1/mm^2]	Healthy	LBR	9.8494	1.30578	7.2901	12.4087
		NLBR	4.0847	0.63369	2.8427	5.3267
		PR	4.9459	0.69700	3.5798	6.3120
	Early OA	LBR	9.4086	0.93164	7.5827	11.2346
		NLBR	4.9227	1.07472	2.8163	7.0292
		PR	4.0273	0.81694	2.4261	5.6285
Feret [μm]	Healthy	LBR	55.0379	1.67731	51.7504	58.3254
		NLBR	74.3126	3.78749	66.8892	81.7359
		PR	91.2981	5.02074	81.4576	101.1385
	Early OA	LBR	75.2642	5.64603	64.1982	86.3302
		NLBR	131.5837	7.26056	117.3532	145.8141
		PR	163.2516	16.30501	131.2944	195.2088
MinFeret [μm]	Healthy	LBR	36.2217	0.91409	34.4301	38.0133
		NLBR	46.5323	2.61515	41.4067	51.6579
		PR	57.5529	3.44594	50.7990	64.3068
	Early OA	LBR	47.9398	6.71750	34.7738	61.1059
		NLBR	89.4938	9.75733	70.3698	108.6178
		PR	95.6795	6.89743	82.161	109.1982
Circ.	Healthy	LBR	0.8318	0.0126	0.807	0.857
		NLBR	0.7522	0.0124	0.737	0.767
		PR	0.6942	0.0104	0.671	0.718
	Early OA	LBR	0.7916	0.026	0.7397	0.8436
		NLBR	0.7103	0.012	0.686	0.734
		PR	0.6675	0.016	0.636	0.702

Table II

Osteoarthritis and Cartilage

Region-specific CMMC metrics in healthy and early OA human femoral heads

readily diagnosable in clinical settings[26]. This is due to the low sensitivity of current non-invasive analytical methods, which makes them inadequate to quantify subtle microarchitectural changes[27]. In subchondral bone, particularly, much is unknown about the direct microstructural pathways that connect AC to the trabecular spacing, and to our knowledge, this is the first study examining early osteoarthritic changes of SB microchannel network in human femoral heads.

High-resolution 3D mapping of SB reveals a complex network of CMMCs that directly connects the medullary cavity and the deep zone of cartilage, where regional differences in the CMMC number and size—irrespective of the health-status of cartilage—seem to reflect regional differences in habitual loading on the joint[16]. This observation may have several biological interpretations: (1) There is evidence that in normal, non-arthritic joints, the areas of higher cartilage thickness and subchondral bone thickness are colocalized[16,20,21,23]. In such regions, the length of the diffusion pathway from the subchondral region to the basal cartilage layer is shorter than that from the cartilage surface[28], which makes it conceivable that the CMMCs have nutritive functions (i.e., O_2 and glucose) at least for deep-lying chondrocytes adjacent to the tidemark[14]. The abundance of the CMMCs in the central areas of the joint that are generally subject to a higher compressive stress can then be interpreted as a functional adaptation for providing adequate nutritive support[20]. Interestingly, the density of microcracks—another possible communication pathway for nutrition and cartilage—bone crosstalk—has been correlated to improved cartilage homeostasis as well[29]. (2) The exchange of pore fluid between the (micro)porous structures of bone due to cyclic mechanical loading and blood pressure has been deemed crucial in nutrient transport[30]. It is also reported that the pressure of deeper layers of the AC can be relayed via fluid shifts[31]. The effect of such pressure fluctuations could, on the one hand, influence the extent and type of nutrient supply, and on the other hand, the formative stimulus on bone cells in the basal layer of the AC[20]. It is therefore plausible that the CMMCs are passages for the interstitial fluid movement between the cartilage and the medullary cavity.

In early OA, the minimum and maximum CMMC size is evidently increased compared to intact-cartilage subjects. At the NLBR and the PR, the significance levels are particularly high, and more pronounced for the maximum size than the minimum size. Given that the CMMC number is unchanged compared to the healthy groups, it can be inferred that the porosity of the SB (number per area*size) is increased in early OA. This result is consistent with reports demonstrating elevation of subchondral plate porosity during early stages of OA development[32,33]. OA induction has been shown to increase osteoclast activity directly below the SB, creating a large increase in the SB porosity[34]. The increase in the size of SB perforations can be interpreted as a compensatory mechanism to enhance bone-cartilage crosstalk for diffusion of small molecules[32,35].

Our data suggest that subchondral bone thickness is more affected by the region of the joint than the cartilage condition. One possible reason for this may be the lower number of early OA measuring points in the LBR, which can reduce the overall effect of cartilage condition. Nonetheless, the reduction of SB thickness is mostly local at the NLBR and the PR of the joint, which can be interpreted as evidence for the increased deterioration of bone in early stages of OA. The early phase of OA is known to be associated with structural deterioration, and an early loss of bone due to elevated bone remodeling[36]. In particular, the subchondral plate shows obvious propensity for thinning as an early response[37,38].

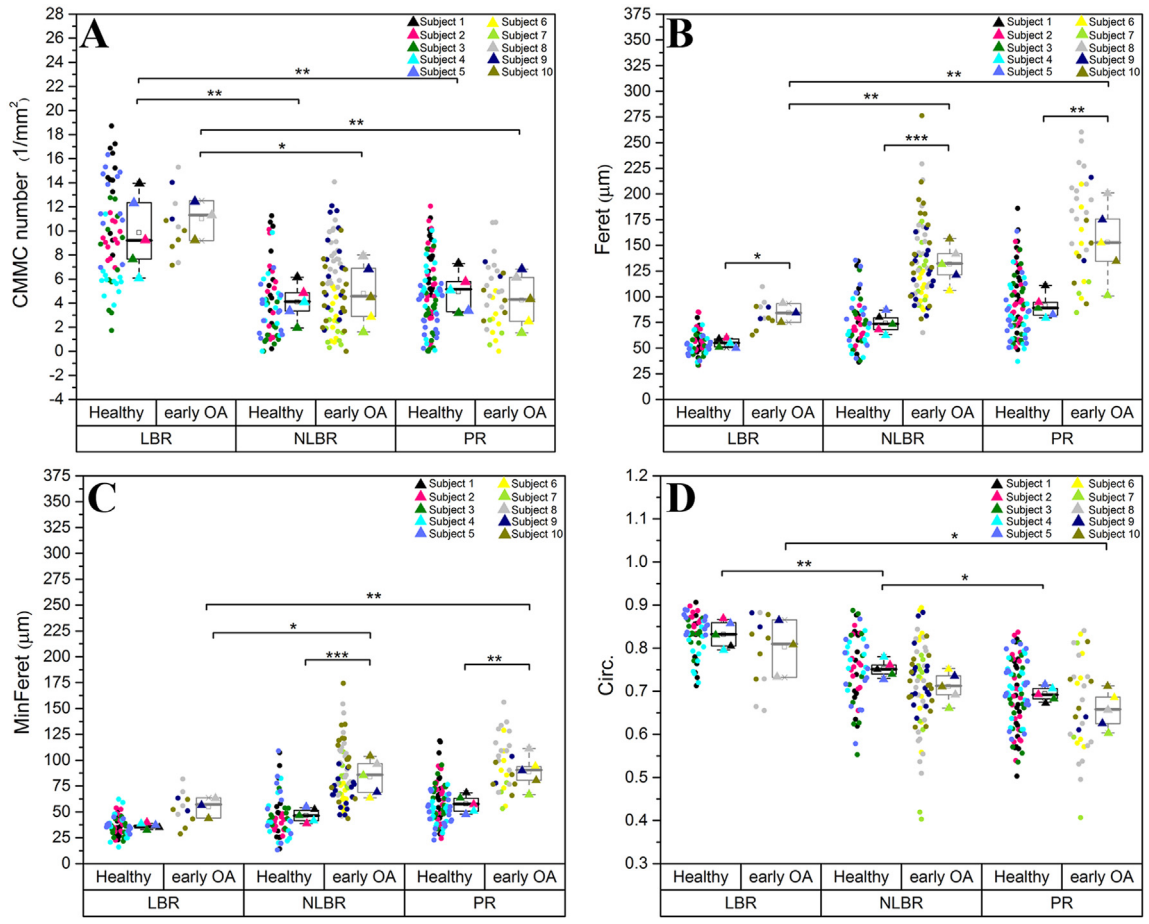

Fig. 5

Osteoarthritis and Cartilage

Quantitative analysis of the CMMC metrics in healthy and early OA human femoral heads. The changes of the (*A*) CMMC number, (*B*) maximum caliper diameter (Feret), (*C*) minimum caliper diameter (MinFeret), and (*D*) the circularity index (Circ.) at the uppermost 50 μm of the SB are depicted as boxplots. The triangles overlying the boxplots denote the mean values of each subject in different loading areas. Subjects 1–5 were healthy while subjects 6–10 had early osteoarthritic chondral characteristics ($n = 5$ per group). Each circle in the immediate proximity to the boxplots represents the mean value of a measuring point, color-coded to its corresponding subject (**m**; number of measuring points = 215 for healthy subjects; 116 for early OA subjects). Analysis was conducted using generalized estimating equation followed by the Bonferroni test for pairwise comparison. Significant *p*-values are presented as *p <0.05; **p <0.01; ***p <0.001.

We found that only ~10% of the affected areas on the femoral heads characterized by early cartilage lesions were located at the LBR, which may be surprising considering the fact that increased chronic loads are seen as major contributors to cartilage damage and degeneration[39,40]. Nonetheless, it is reported that early cartilage fibrillation and splitting is more commonly seen at the edges of the joint contact regions or at the inferomedial portion of the human femoral head, even though SB exposure in end-stage OA patients usually develops on or near the central, LBRs[36,41–43]. This paradox has puzzled some scientists and led them to believe that focal chondral defects on the inferomedial portion have a small capacity to progress into full SB exposure, while those located superocentrally, have a higher osteoarthritic potential, even though they are less frequent[44]. It is, thus, equivocal whether partial-thickness chondral lesions are as relevant in the context of OA progression as full-thickness defects. Nevertheless, it has been demonstrated that regardless of defect depth, the prevalence of focal cartilage defects in an isolated sub-region of the tibiofemoral joint increases the risk for development of new chondral defects in unaffected sub-regions of the same joint[45]. Local investigation of partial-thickness chondral lesions and its underlying SB are, therefore, important when exploring preventive measurements or repair strategies of degenerative changes, which possibly should target non-load-bearing and the peripheral areas of the joint[46,47].

Our preliminary histological analysis shows that most CMMCs have some type of soft-tissue content, e.g., tunica intima with cell linings at their basement membrane. It is frequently reported that at least some of the SB perforations are conduits for blood vessels that are lined by endothelium[14,48]. These thin-walled vessels contain elements of the peripheral blood such as erythrocytes [Fig. S6(G)], and are engulfed by concentric layers of bone. Our histological observations, however, point to a much more heterogeneous profile of possible CMMC contents such as small (12–25 μm) and medium-sized (35–55 μm) capillaries, sinusoids,

post-capillary venules and arterioles-like structures. These contents may have important implications in bone (patho)physiology, e.g., to allow for the diffusion-driven exchange of nutrients, mediators, growth factors, and waste products in blood and/or the interstitial fluid[18,28,49]. Dedicated and comprehensive studies are needed to evaluate the precise CMMC contents and their quantitative variations regarding the effect of region and cartilage condition. Additionally, it would be interesting to examine possible correlations of CMMCs with those characteristics of the overlying cartilage that typify OA progression, e.g., the percentage of the tidemark duplication length to that of local cartilage thickness.

A limitation of our study is the small sample size in each group ($n = 5$) and the unknown medical history of the human cadavers. Nonetheless, the biopsy-based mapping of the CMMCs across the entire femoral head at an isotropic voxel size of 1.2 μm was inherently restricting. i.e., for a reasonably higher sample size (e.g., $n = 10$ per group), either twice as much biopsies would have had to be scanned, which was simply inconceivable given the time needed for scanning and more importantly data processing. Or a compromise would have had to be made in terms of the distance between individual measuring points (i.e., the mapping detail). Here, we decided to give the priority to the mapping detail owing to the high intra-regional variance that was expected, as well as the fact that an imprecise perception of the CMMC characteristics could potentially jeopardize ongoing/future studies on pathological joints, or cause misinterpretations. Therefore, we hope that the small sample size of this study can be evaluated in a context-dependent manner. Another limitation is the evaluation of the CMMC metrics in sequential 2D layers rather than in three-dimensional models. Hence, Feret. and Circ. may also reflect the angle at which the microchannels run through the SB, as slanted channels are cut by a transverse plane of sectioning, which can possibly lead to an overestimation of the values. However, at the uppermost 50 μm of the AC-SB interface where the values are computed, the channels have to merge to the SB surface and are therefore perpendicularly extended, which minimizes this potential effect.

In conclusion, we have profiled and evaluated the influence of cartilage condition as well as local regions of human femoral head on SB microarchitecture in early idiopathic OA. Our findings point to a previously undescribed enlargement of the SB microchannel network especially in the unloaded region of the joint, and a collective structural deterioration of SB in early stages of OA. Still, the AC-SB interface seems to be even more intricate than originally thought, and several questions regarding the functionality and the cellular/molecular content of the CMMCs remain to be answered. Likewise, it would be interesting to assess the evolution of CMMCs during the late-stages of the pathological cycle. Given the biphasic nature of OA progression[36], and the sclerotic response of SB in end-stage OA[50], a remodeling sequence may be hypothesized in which the subchondral densification and excessive bone matrix formation occlude the connective pathways between the medullary cavity and the basal layer of cartilage. This can be used as a direction for future research.

Data availability

The data that support the findings of this study are available from the corresponding author (ST) upon reasonable request.

Informed consent

Bone tissue samples were derived from the anatomical gift program of the MHH, and thus all the participants signed the consent form for the whole-body donation executed by the prospective donor.

Author contributions

Conceptualization, ST and AFS; Data curation, ST, TY, RHF, LJ, and ALF; Formal analysis, ST, TY, KOB, RHF, LJ, ALF, and BG; Funding acquisition, WL and AFS; Investigation, ST, TY, KOB, RHF, LJ, ALF, and BG; Methodology, ST, TY, KOB, ALF, BG, TH, WL, and AFS; Project administration, ST and AFS; Resources, WL and AFS; Supervision, AFS; Validation, ST, TY, ALF, TH, BG; Visualization, ST and TY; Writing – original draft, ST, TY, ALF; Writing – review & editing, ST, TY, KOB, RHF, LJ, ALF, BG, TH, WL and AFS.

Conflict of interest

Shahed Taheri and Arndt Friedrich Schilling have filed a patent application with the University Medical Center Göttingen that is partially based on the results reported in the current manuscript. All other authors have nothing to disclose.

Funding

This study was supported by the German Research Foundation (DFG) as part of subproject 5 [SCHI 857/9-1/SCHI 857/9-2] of the Research Consortium ExCarBon FOR2407.

Acknowledgments

The authors would like to thank the anonymous body donors and the Prosektur of the Institute for Functional and Applied Anatomy for their donation of the bone samples. Likewise, we would like to thank Timo Beil and Jan Hubert for classification of the bones according to the Outerbridge system, and Andreas Buchhorn (MHH) for his support with the samples.

Supplementary data

Supplementary data to this article can be found online at https://doi.org/10.1016/j.joca.2022.10.002.

References

1. Latourte A, Kloppenburg M, Richette P. Emerging pharmaceutical therapies for osteoarthritis. Nat Rev Rheumatol 2020 Oct 29;16(12):673–88.
2. Loeser RF, Goldring SR, Scanzello CR, Goldring MB. Osteoarthritis: a disease of the joint as an organ. Arthritis Rheum 2012 Jun;64(6):1697–707.
3. Onishi K, Utturkar A, Chang E, Panush R, Hata J, Perret-Karimi D. Osteoarthritis: a critical review. Crit Rev Phys Rehabil Med 2012;24(3–4):251–64.
4. Castañeda S, Roman-Blas JA, Largo R, Herrero-Beaumont G. Subchondral bone as a key target for osteoarthritis treatment. Biochem Pharmacol 2012;83:315–23. Elsevier.
5. Li G, Yin J, Gao J, Cheng TS, Pavlos NJ, Zhang C, *et al*. Subchondral bone in osteoarthritis: insight into risk factors and microstructural changes. Arthritis Res Ther 2013;15(6):223.
6. Yuan XL, Meng HY, Wang YC, Peng J, Guo QY, Wang AY, *et al*. Bone–cartilage interface crosstalk in osteoarthritis: potential pathways and future therapeutic strategies. Osteoarthritis Cartilage 2014 Aug;22(8):1077–89.
7. Shang X, Böker KO, Taheri S, Lehmann W, Schilling AF. Extracellular vesicles allow epigenetic mechanotransduction between chondrocytes and osteoblasts. Int J Mol Sci 2021 Dec 10;22(24), 13282.
8. Lajeunesse D, Reboul P. Subchondral bone in osteoarthritis: a biologic link with articular cartilage leading to abnormal remodeling. Curr Opin Rheumatol 2003;15:628–33.
9. Bellido M, Lugo L, Roman-Blas JA, Castañeda S, Caeiro JR, Dapia S, *et al*. Subchondral bone microstructural damage by

increased remodelling aggravates experimental osteoarthritis preceded by osteoporosis. Arthritis Res Ther 2010 Aug 2;12(4).
10. Henrotin Y, Pesesse L, Sanchez C. Subchondral bone and osteoarthritis: biological and cellular aspects. Osteoporos Int 2012 Dec;23(8 Suppl).
11. Greenwald AS, Haynes DW. A pathway for nutrients from the medullary cavity to the articular cartilage of the human femoral head. J Bone Joint Surg Br 1969 Nov;51(4):747–53.
12. Hodge JA, McKibbin B. The nutrition of mature and immature cartilage in rabbits. An autoradiographic study. J Bone Joint Surg Br 1969 Feb 1;51(1):140–7.
13. Holmdahl DE, Ingelmark BE. The contact between the articular cartilage and the medullary cavities of the bone. Acta Orthop Scand 1950;20(2):156–65.
14. Duncan H, Jundt J, Riddle JM, Pitchford W, Christopherson T. The tibial subchondral plate. A scanning electron microscopic study. J Bone Joint Surg Am 1987 Oct;69(8):1212–20.
15. Taheri S, Winkler T, Schenk L, Neuerburg C, Baumbach S, Zustin J, *et al*. Developmental transformation and reduction of connective cavities within the subchondral bone. Int J Mol Sci 2019 Feb 12;20(3):770.
16. Taheri S, Yoshida T, Böker KO, Foerster RH, Jochim L, Flux AL, *et al*. Investigating the microchannel architectures inside the subchondral bone in relation to estimated hip reaction forces on the human femoral head. Calcif Tissue Int 2021 Nov 1;109(5):510–24.
17. Taheri S, Böker KO, Lehmann W, Schilling AF. Knorpel-Knochenmark-Mikro-Konnektoren im subchondralen Knochen. Osteologie 2021 Feb 1;30(1):13–20.
18. Lyons TJ, McClure SF, Stoddart RW, McClure J. The normal human chondro-osseous junctional region: evidence for contact of uncalcified cartilage with subchondral bone and marrow spaces. BMC Musculoskelet Disord 2006 Jun 20;7(1):52.
19. Findlay DM, Kuliwaba JS. Bone–cartilage crosstalk: a conversation for understanding osteoarthritis. Bone Res 2016 Dec 20;4(1), 16028.
20. Milz S, Putz R. Lückenbildungen der subchondralen Mineralisierungszone des Tibiaplateaus. Osteologie 1994;3(4):110–8.
21. Woods CG, Greenwald AS, Haynes DW. Subchondral vascularity in the human femoral head. Ann Rheum Dis 1970;29(2):138–42.
22. Ogata K, Whiteside LA, Lesker PA. Subchondral route for nutrition to articular cartilage in the rabbit. Measurement of diffusion with hydrogen gas in vivo. J Bone Joint Surg Am 1978 Oct;60(7):905–10.
23. Clark JM. The structure of vascular channels in the subchondral plate. J Anat 1990;171:105–15.
24. Burr DB. The importance of subchondral bone in osteoarthrosis. Curr Opin Rheumatol 1998 May;10(3):256–62.
25. Quasnichka HL, Anderson-MacKenzie JM, Bailey AJ. Subchondral bone and ligament changes precede cartilage degradation in Guinea pig osteoarthritis. Biorheology 2006;43(3,4):389–97.
26. Emery CA, Whittaker JL, Mahmoudian A, Lohmander LS, Roos EM, Bennell KL, *et al*. Establishing outcome measures in early knee osteoarthritis. Nat Rev Rheumatol 2019 Jun 14;15(7):438–48.
27. Mastbergen SC, Lafeber FPJG. Changes in subchondral bone early in the development of osteoarthritis. Arthritis Rheum 2011 Sep 1;63(9):2561–3.
28. Imhof H, Breitenseher M, Kainberger F, Trattnig S. Degenerative joint disease: cartilage or vascular disease? Skeletal Radiol 1997 Jul 7;26(7):398–403.
29. Zarka M, Hay E, Ostertag A, Marty C, Chappard C, Oudet F, *et al*. Microcracks in subchondral bone plate is linked to less cartilage damage. Bone 2019 Jun 1;123:1–7.
30. Wittkowske C, Reilly GC, Lacroix D, Perrault CM. In vitro bone cell models: impact of fluid shear stress on bone formation. Front Bioeng Biotechnol 2016 Nov 15;4:87.
31. Occhetta P, Mainardi A, Votta E, Vallmajo-Martin Q, Ehrbar M, Martin I, *et al*. Hyperphysiological compression of articular cartilage induces an osteoarthritic phenotype in a cartilage-on-a-chip model. Nat Biomed Eng 2019 Jul 3;3(7):545–57.
32. Hwang J, Bae WC, Shieu W, Lewis CW, Bugbee WD, Sah RL. Increased hydraulic conductance of human articular cartilage and subchondral bone plate with progression of osteoarthritis. Arthritis Rheum 2008;58(12):3831–42.
33. Intema F, Hazewinkel HAW, Gouwens D, Bijlsma JWJ, Weinans H, Lafeber FPJG, *et al*. In early OA, thinning of the subchondral plate is directly related to cartilage damage: results from a canine ACLT-meniscectomy model. Osteoarthritis Cartilage 2010 May;18(5):691–8.
34. Botter SM, Van Osch GJVM, Clockaerts S, Waarsing JH, Weinans H, Van Leeuwen JPTM. Osteoarthritis induction leads to early and temporal subchondral plate porosity in the tibial plateau of mice: an in vivo microfocal computed tomography study. Arthritis Rheum 2011 Sep;63(9):2690–9.
35. Pan J, Wang B, Li W, Zhou X, Scherr T, Yang Y, *et al*. Elevated cross-talk between subchondral bone and cartilage in osteoarthritic joints. Bone 2012 Aug;51(2):212–7.
36. Burr DB, Gallant MA. Bone remodelling in osteoarthritis. Nat Rev Rheumatol 2012;8:665–73.
37. Meyer EG, Baumer TG, Slade JM, Smith WE, Haut RC. Tibiofemoral contact pressures and osteochondral microtrauma during anterior cruciate ligament rupture due to excessive compressive loading and internal torque of the human knee. Am J Sports Med 2008:1966–77.
38. Sniekers YH, Intema F, Lafeber FPJG, Van Osch GJVM, Van Leeuwen JPTM, Weinans H, *et al*. A role for subchondral bone changes in the process of osteoarthritis; A micro-CT study of two canine models. BMC Musculoskelet Disord 2008 Dec 12;9(1):20.
39. Goldring MB, Goldring SR. Articular cartilage and subchondral bone in the pathogenesis of osteoarthritis. Ann N Y Acad Sci 2010:230–7. Blackwell Publishing Inc.
40. Roemhildt ML, Coughlin KM, Peura GD, Badger GJ, Churchill D, Fleming BC, *et al*. Effects of increased chronic loading on articular cartilage material properties in the Lapine tibiofemoral joint. J Biomech 2010 Aug;43(12):2301–8.
41. Meachim G, Whitehouse GH, Pedley RB, Nichol FE, Owen R. An investigation of radiological, clinical and pathological correlations in osteoarthrosis of the hip. Clin Radiol 1980 Jan 1;31(5):565–74.
42. Meachim G, Emery IH. Cartilage fibrillation in shoulder and hip joints in Liverpool necropsies. J Anat 1973 Nov;116(Pt 2):161–79.
43. Meachim G, Allibone R. Topographical variation in the calcified zone of upper femoral articular cartilage. J Anat 1984 Sep;139(Pt 2):341–52.
44. Byers PD, Contepomi CA, Farkas TA. A post mortem study of the hip joint. Including the prevalence of the features of the right side. Ann Rheum Dis 1970;29(1):15–31.
45. Guermazi A, Hayashi D, Roemer FW, Niu J, Quinn EK, Crema MD, *et al*. Partial- and full-thickness focal cartilage defects contribute equally to development of new cartilage damage in knee osteoarthritis: the multicenter osteoarthritis study. Arthritis Rheumatol 2017 Mar 1;69(3):560–4.
46. Jansen EJ, Emans PJ, Van Rhijn LW, Bulstra SK, Kuijer R. Development of partial-thickness articular cartilage injury

in a rabbit model. Clin Orthop Relat Res 2008;466(2):487–94.
47. Schilling AF, Taheri S. In: Microchannels in Subchondral Bone and Membranes Comprising Same for the Treatment of Osteoarthritis, Vol. US20210298. DE: USPTO; 20211–31.
48. Clark JM, Huber JD. The structure of the human subchondral plate. J Bone Joint Surg Br 1990 Sep;72(5):866–73.
49. Huang Y, Chen C, Wang F, Chen G, Cheng S, Tang Z, *et al*. Observation of solute transport between articular cartilage and subchondral bone in live mice. Cartilage 2021 Dec 1;13(2 Suppl):398S–407S.
50. Madry H, van Dijk CN, Mueller-Gerbl M. The basic science of the subchondral bone. Knee Surg Sports Traumatol Arthrosc 2010;18(4):419–33.